



1 **Three dominant synoptic atmospheric circulation**
2 **patterns influencing severe winter haze in eastern China**

3 Shiyue Zhang¹, Gang Zeng^{1*}, Tijian Wang², Xiaoye Yang¹, Vedaste Iyakaremye³

4 ¹Key Laboratory of Meteorological Disaster, Ministry of Education, Collaborative Innovation Center on
5 Forecast and Evaluation of Meteorological Disasters (CIC-FEMD), Joint International Research
6 Laboratory of Climate and Environment Change (ILCEC), Nanjing University of Information Science
7 and Technology, Nanjing, China, 210044

8 ²School of Atmospheric Sciences, Nanjing University, Nanjing, 210023, China

9 ³Rwanda Meteorology Agency, Nyarugenge KN 96 St, Kigali, Rwanda

10

11 *Correspondence to: Gang Zeng (zenggang@nuist.edu.cn)*

12

13 **Abstract.** Previous studies indicated that, on synoptic scale, the severe haze in eastern China (EC)
14 is affected by the atmospheric circulation variations. However, it is still unclear what are the
15 dominant atmospheric circulation patterns influencing the severe winter haze conditions in EC and
16 what are the differences between them. To systematically determine the dominant synoptic
17 atmospheric circulation patterns of severe haze in different regions of EC, we use the Hierarchical
18 Clustering Algorithm to classify the local geopotential height anomalies at 500-hPa over the stations
19 with severe haze and obtained three dominant synoptic atmospheric circulation types based on
20 observed PM_{2.5} concentration and NCEP/NCAR reanalysis. Circulation Type1 is accompanied by
21 significant north wind component anomalies over northern China and causes severe haze pollution
22 over the Yangtze River valley. Although the local meteorological conditions are not conducive to
23 haze formation and accumulation, the severe haze in Yangtze River valley is related to the pollution
24 transportation caused by the north wind anomalies. During the haze days with circulation Type2,
25 the joint affection of East Atlantic-West Russia teleconnection pattern and winter East Asia
26 subtropical jet stimulate and maintain the anticyclonic anomalies over northeast Asia, which
27 provides meteorological conditions conducive to the occurrence of severe haze over the whole EC.
28 The circulation Type3 mainly caused severe haze events in northeast China through the
29 establishment of blocking high over the Okhotsk Sea. The results provide a basis for establishing
30 haze prediction and management policies applicable to different regions in EC.



31 1. Introduction

32 Severe haze could increase the risk of traffic accidents by reducing visibility and harm human
33 health by causing respiratory diseases (Xie et al., 2014; Hu et al., 2015; Wang et al., 2016). Haze
34 events in China are mainly caused by PM_{2.5} (particulate with an aerodynamic diameter less than
35 2.5µm; Cai et al., 2017; Shen et al., 2018; Wang et al., 2021). Researches show that the distribution
36 of haze days in China has the characteristics of uneven spatial distribution, with more in
37 economically developed eastern region and less in economically underdeveloped region (Wu et al.,
38 2013; Liu et al., 2015; Xu et al., 2015). With the rapid development of industrialization, urbanization
39 and increase in anthropogenic emission, eastern China (EC) has experienced more severe haze
40 events with long duration, large spatial scale, and serious harm in the past few decades (Monks et
41 al., 2009; Qian et al., 2009; Wang et al., 2009). Since the beginning of the 21st century, the uneven
42 spatial distribution of haze events in China have become more obvious (Sun et al., 2016), which has
43 led to the increasing incidence rate and mortality related to respiratory diseases in Beijing-Tianjin-
44 Hebei, the Yangtze River valley, and the Pearl River Delta (Tsaia et al., 2014; Ding et al., 2016; Fan
45 et al., 2019). Although haze pollution control in China has been improved to some extent with the
46 strict implementation of energy conservation and emission reduction policies after 2013 (Wang et
47 al., 2021), it still affects various socio-economic sectors and human health.

48 In addition to human activities, meteorological conditions are also considered as one of the most
49 important factors for determining regional air quality. Previous studies have indicated that, on the
50 weather scale, the formation and maintenance of haze days in eastern China (HD_{EC}) are closely
51 related to favorable weather conditions (Niu et al., 2010; Cai et al., 2017), including strong thermal
52 inversion potential, high relative humidity, negative sea level pressure anomaly, and weak wind
53 speed. Furthermore, the anticyclonic anomaly could lead to the sinking movement and weaker
54 thermal inversion potential, which inhibit the vertical diffusion of pollutants and affect the air quality
55 of the local or larger region (Wu et al., 2013; Xu et al., 2015). Many studies investigated the key
56 circulation system affecting HD_{EC} from an interannual scale or intraseasonal scale and suggested
57 that the weak East Asian Winter Monsoon (Li et al., 2015; Yin et al., 2015; Zhang et al., 2022), the
58 positive phase of Arctic Oscillation (Wang et al., 2015; Yin et al., 2015) and the positive phase of
59 East Atlantic-West Russia (EA/WR) teleconnection pattern (Yin et al., 2017) could result in more



60 haze days in China. On the synoptic scale, meteorological conditions could also significantly
61 regulate HD_{EC} . The weak synoptic circulation with a high-pressure or continuous low-pressure
62 system is beneficial for the accumulation of pollution, while the strong weather phenomena with a
63 large pressure gradient encourage the diffusion of pollutants (Li et al., 2019; Cai et al., 2020).
64 Furthermore, studies have shown that cold surges can dissipate and reduce local air pollutants by
65 bringing dry and clean cold air (Wu et al., 2017; Leung et al., 2018; Zhang et al., 2021).

66 A recent study classified the daily winter circulation anomalies and suggested that there are two
67 dominant climate drivers (i.e., EA/WR teleconnection pattern and Victoria mode of sea surface
68 temperature anomalies) conducive to the severe haze occurrence in North China (Li et al., 2022).
69 However, there is still a lack of research on the dominant circulation patterns of severe HD_{EC} .
70 Therefore, the present study addresses the following scientific questions: (1) what are the synoptic
71 atmospheric circulation patterns that dominate severe haze pollution in EC, (2) what are the
72 differences in the action range of each circulation pattern, and what are their possible mechanisms.
73 These issues are addressed using a modified classification algorithm (Hierarchical Clustering
74 Algorithm) that is more suitable for studying the classification of synoptic patterns in a large spatial
75 range.

76 The remaining sections of this paper are structured as follows: Data and definitions are
77 introduced in section 2. Section 3 shows the dominant synoptic circulation patterns of severe HD_{EC} .
78 In section 4, we compare different circulation types associated with severe HD_{EC} . Finally, the
79 discussion and main conclusions are given in section 5.

80 **2. Data and Methods**

81 **2.1 Data**

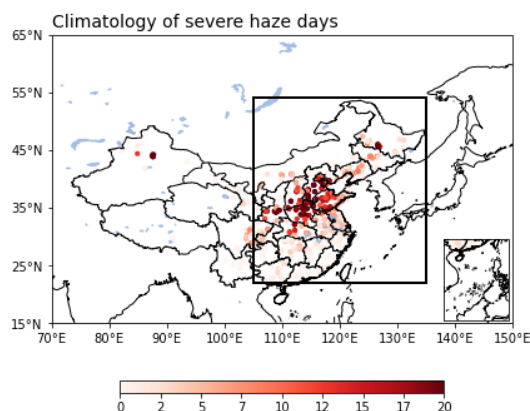
82 In this study, the daily meteorological data and the observed $PM_{2.5}$ concentrations from 2014 to
83 2021 were used to analyze the dominant circulation patterns and their main causes of severe haze
84 in winter in EC. The daily NCEP/NCAR reanalysis was obtained from <https://psl.noaa.gov/>, which
85 includes sea level pressure (SLP), surface air temperature (SAT), the temperature in multiple
86 pressure levels, geopotential height (GPH), three-dimensional wind, relative humidity (RH) at 1000-



87 hPa, and vertical velocity (ω) at 850-hPa (Kalnay et al., 1996). The dataset has a horizontal
88 resolution of $2.5^\circ \times 2.5^\circ$. In this study, we defined the thermal inversion potential (TIP) as the air
89 temperature at 850-hPa minus SAT referring to Yin and Wang (2019). The Daily $PM_{2.5}$ concentrations
90 for 935 meteorological stations in China (following Yin and Wang (2016) and Yin et al. (2021), the
91 stations with missing data more than 5% of are dropped; the stations with data lost continuously for
92 3 days or more is also discarded) were obtained from China National Environmental Monitoring
93 Centre (<https://quotsoft.net/air/>). The sporadic missing data (less than 3 days) were filled by cubic
94 spline interpolation.

95 2.2 Definition of severe HD_{EC}

96 In this study, the severe HD_{EC} is defined when $PM_{2.5}$ concentration $\geq 150 \mu\text{g m}^{-3}$ (Cai et al., 2017;
97 Zhong et al., 2019). We focused on the haze days in the cool season (November to February of the
98 following year, abbreviated as NDJF), which accounts for more than 40% of the total haze days in
99 China in a year (Sun et al., 2013; Wang et al., 2015). Figure 1 shows the climatology of haze days
100 in China from 2014 to 2021 in NDJF. The severe haze days are mainly concentrated in the EC (east
101 of 105°E and south of 54°N), which is selected as the target area in the present study. Thus, a subset
102 of 853 stations is selected.



103

104 **Figure 1.** Spatial distribution of the annual averaged severe haze days (unit: day) in China from
105 2014 to 2021 in NDJF. The black box represents EC.



106 2.3 Definition of blocking index

107 In winter, the anticyclone anomaly over the Okhotsk Sea, usually related to atmospheric
108 blocking, may lead to haze accumulation (Yun and Yoo 2019; Hwang et al., 2022). Thus, based on
109 previous studies (Tibaldi et al., 1990; Fang and Lu, 2020), here we identify the blockings by
110 northward gradients (GHGN) and southward gradients (GHGS) of Z_{500} at each grid point:

$$111 \quad GHGN = \frac{z_{500}(\lambda, \phi + \Delta\phi) - z_{500}(\lambda, \phi)}{\Delta\phi} \quad (1)$$

$$112 \quad GHGS = \frac{z_{500}(\lambda, \phi) - z_{500}(\lambda, \phi - \Delta\phi)}{\Delta\phi} \quad (2)$$

113 Where $\phi = 35^\circ, 35.5^\circ \dots, 75^\circ\text{N}$, $\lambda = 70^\circ, 70.5^\circ \dots, 160^\circ\text{E}$ and $\Delta\phi = 15^\circ$. A given longitude is
114 defined as “blocked” at a particular time satisfies the following conditions:

$$115 \quad GHGS > 0, \quad GHGN < -10 \text{ m (deg lat)}^{-1}$$

116 Based on these conditions, we can identify whether any grid in the range of 35°N - 70°N is blocked
117 at any time.

118 2.4 Plumb's wave activity flux

119 Here we used the wave flux of Rossby to show the propagation of wave energy (Plumb, 1985).
120 The two-dimensional Plumb's wave activity flux can be expressed by:

$$121 \quad F_s = \frac{P}{P_0} \cos \varphi \times \left(\begin{array}{l} v'^2 - \frac{1}{2\Omega a \sin 2\varphi} \frac{\partial(v'\phi')}{\partial\lambda} \\ -u'v' + \frac{1}{2\Omega a \sin 2\varphi} \frac{\partial(u'\phi')}{\partial\lambda} \end{array} \right) \quad (3)$$

122 In Eq. (3), F_s (unit: $\text{m}^2 \text{s}^{-2}$) denotes the horizontal stationary wave activity flux, P means the
123 pressure; $P_0 = 1000\text{-hPa}$, u' and v' are the zonal and meridional wind deviation, respectively.
124 And the ϕ' is geopotential height. φ (λ) represents the latitude (longitude). a is the radius of Earth,
125 and Ω means Earth's rotation rate.

126

127 2.5 Classification algorithm of synoptic atmospheric circulation

128 This paper uses the hierarchical clustering algorithm (HCA) to classify the severe HD_{EC} based
129 on the associated circulations anomalies. Based on HCA (Rokach et al., 2005), we could create a
130 clustering tree of data samples by calculating the Euclidean distance between different categories.



131 The original data samples of different types are at the lowest level of the tree, and the root point of
132 a cluster is at the top level of the tree.

133 Unlike Li et al. (2022), we only cluster the circulation anomalies of days with severe HD_{EC},
134 which can ensure that all classification samples lead to PM_{2.5} at least one station in EC exceeds the
135 standard of severe haze pollution and produce more accurate classification types. Secondly, the
136 circulation samples selected are not in fixed region, but the rectangular regions of the same size
137 centered on each station with severe haze (the GPH anomalies at 500-hPa in a rectangular region of
138 30 degrees from east, west, north, and south with each station as the center on the day of severe
139 HD_{EC} were taken as the samples to perform HCA). It means that our classification results are
140 focused on the local circulation anomalies accompanied by haze.

141 We use the silhouette coefficient to determine the optimal classification result (Rousseeuw,
142 1987). For any sample i , the silhouette coefficient $s(i)$ is defined as:

$$143 \quad s(i) = \frac{b(i) - a(i)}{\max\{a(i), b(i)\}} \quad (4)$$

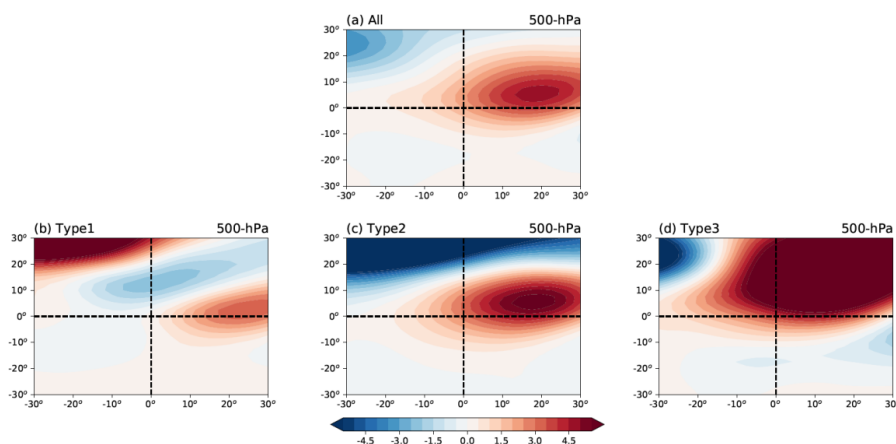
144 $a(i)$ means the average distance from sample i to all other samples in the cluster it belongs to,
145 and $b(i)$ means the lowest average distance from sample i to all samples in any other cluster. The
146 silhouette coefficient of the clustering result is the average of the silhouette coefficients of all
147 samples. The closer to 1, the better the classification results. Figure S1 shows the clustering tree and
148 its associated silhouette coefficient of this study.

149 3. Dominant synoptic atmospheric circulation patterns of severe HD_{EC}

150 Figure 2a shows the composite anomalies of 500-hPa GPH during all severe HD_{EC} in 853
151 stations. Generally, the stations with severe haze are located in the southwestern parts of the
152 anticyclonic anomaly center, which is consistent with previous studies (Zhong et al., 2019; Wang
153 and Zhang, 2020). Then we performed the HCA as described in Section 2.5 and obtained three types
154 of dominant local circulation anomalies associated with the severe HD_{EC} (Figure 2b, c, d).
155 Circulation Type1 shows a wave-train structure of '+ - +', and the stations are located in the west
156 of anticyclonic anomaly and the south of cyclonic anomaly. Circulation Type2 shows the circulation
157 anomalies similar to Figure 2a. Finally, circulation Type3 denotes that the stations are located south
158 of the anticyclonic anomaly, and the intensity and range of the anticyclonic anomaly are



159 significantly stronger than the other two patterns. The differences between the types imply that
160 severe HD_{EC} may be related to different causes.

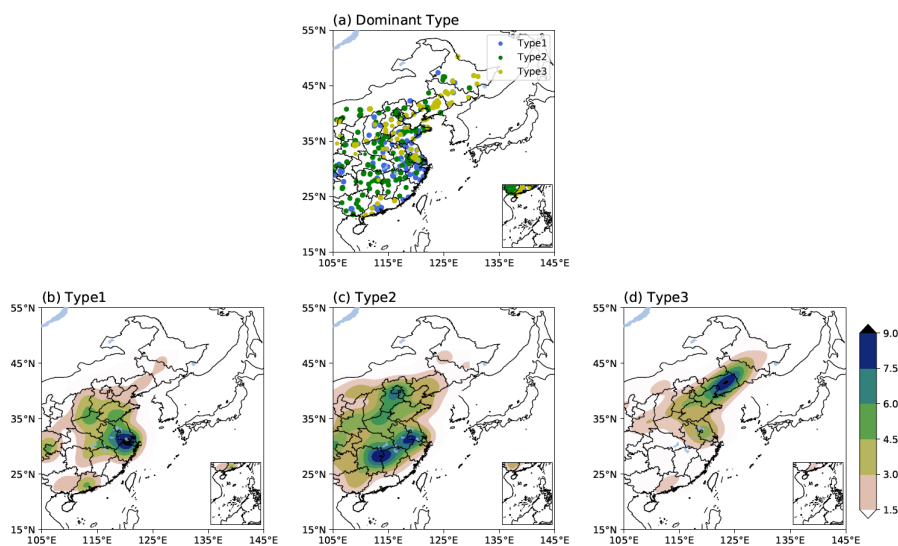


161

162 **Figure 2.** (a) Composite anomalies of GPH at 500-hPa (units: gpm) during all severe HD_{EC} in 853
163 stations. (0°, 0°) represents the location of stations. (b), (c), and (d) are same as (a) but for three sub-
164 types.

165

166 For each station, when the probability of a certain circulation type is greater than the sum of
167 the other two types, we define this type as the dominant type of the station. Figure 3 shows the
168 leading circulation types of severe HD_{EC} for 853 stations and the weighted probability density
169 distribution of three circulation types (the weight of each station is the probability of the
170 corresponded dominant type occurring at the station). Stations dominated by the circulation Type1
171 are mainly distributed in the Yangtze River valley (YRV). The stations dominated by the circulation
172 Type2 cover almost the whole EC, with two centers in South China (SC) and Beijing-Tianjin-Hebei
173 region. The stations dominated by the circulation Type3 are mainly located in Northeast China
174 (NEC). These results suggest significant differences in the circulation patterns of severe haze in
175 different regions of EC.

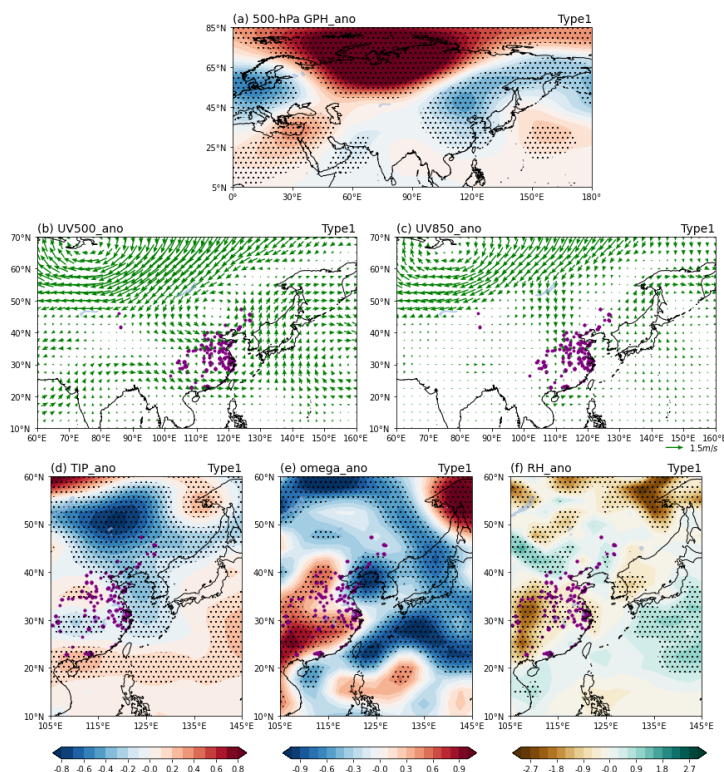


176

177 **Figure 3.** (a) The leading synoptic circulation type of severe HD_{EC} for 853 stations. Weighted
178 probability density distribution of stations dominated by (b) Type1, (c) Type2, and (d) Type3.

179 4. Comparison of different circulation types associated with severe HD_{EC}

180 Figure 4a, b, and c show the composite anomalies of circulation Type1 at 500-hPa and 850-hPa.
181 The circulation Type1 is associated with the upper troposphere's wave-train structure of “- + -”.
182 Unlike previous studies (Zhong et al., 2019; Wang and Zhang, 2020), there are no significant
183 anticyclonic anomalies in the mid-troposphere over YRV, but with substantial north wind
184 component in the lower troposphere over northern China. The TIP, sinking movement, and RH
185 anomalies over the YRV are weak (Figure 4d, e, f). Therefore, it can be inferred that it is not the
186 local circulation anomalies that promote the formation and accumulation of haze pollution, but the
187 regional haze transportation caused by the north wind component anomalies that leads to the severe
188 haze in the YRV.



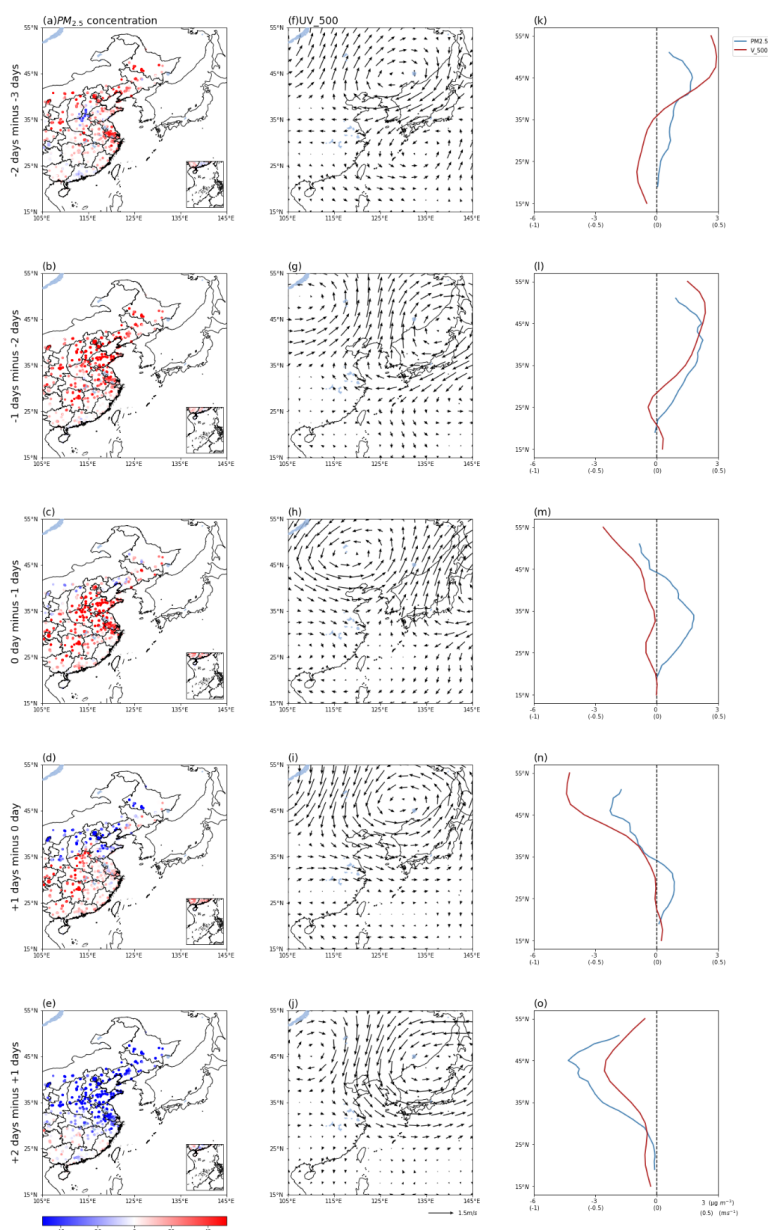
189
190 **Figure 4.** Composite anomalies of (a) GPH at 500-hPa (unit: gpm), horizontal wind (unit: m s^{-1}) at
191 (b) 500-hPa and (c) 850-hPa, (d) TIP (unit: K), (e) omega (unit: $10^{-2} \text{ Pa s}^{-1}$), and (f) RH (unit: %)
192 for circulation Type1. Dotted areas are statistically significant at the 95% confidence level. The
193 purple dots represent the stations dominated by circulation Type1.

194

195 To further explore the relationship between Type1 severe HD_{EC} and north wind component
196 anomalies, we present the evolution of $\text{PM}_{2.5}$ concentration variations ($\text{PM}_{2.5}$ concentration on Day_i
197 minus that on Day_{i-1}) from -3 days to 2 days of Type1 severe HD_{EC} occur (Figure 5a, b, c, d, e) and
198 the corresponding horizontal wind variations at 500-hPa (Figure 5 f, g, h, i, j). $\text{PM}_{2.5}$ concentration
199 tends to increase at first and then dissipate showing an obvious transportation process from north to
200 south. Accordingly, the horizontal wind changes from anticyclonic anomalies to cyclonic anomalies,
201 with the south wind turning to the north wind. Here we average the $\text{PM}_{2.5}$ concentration variations
202 in Figure 5a, b, c, d, e, and meridional wind variations in Figure 5f, g, h, i, j along latitudes (Figure
203 5k, l, m, n, o). The result shows that $\text{PM}_{2.5}$ concentration gradually increased from north EC to south



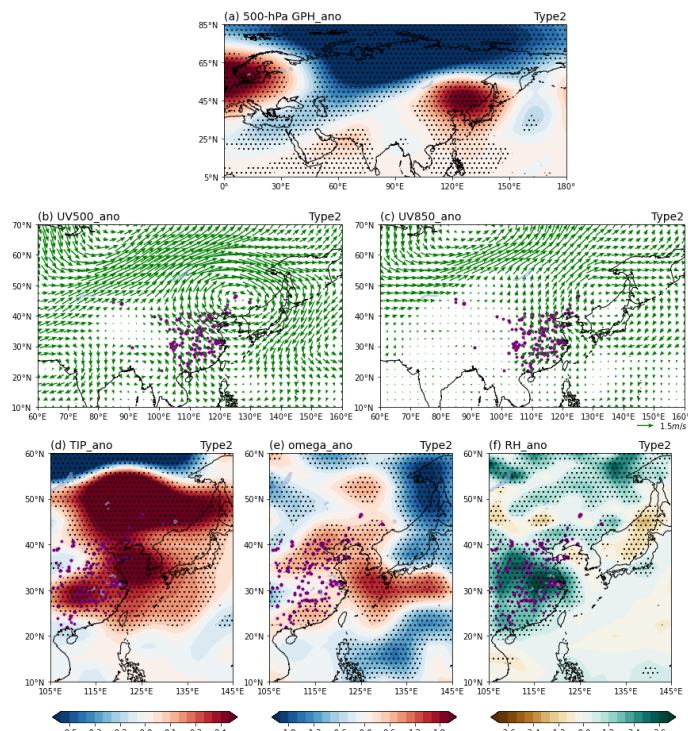
204 EC and began to decrease after severe HD_{EC} occurred. With the variation in PM_{2.5} concentration,
 205 the south wind in the north EC gradually weakens and turns to the north wind when severe HD_{EC}
 206 occurs. With the dry and cold air from the north invading southward, the haze dissipates rapidly,
 207 and EC can maintain high air quality weather. Therefore, although circulation Type1 will lead to
 208 severe haze in YRV, its circulation anomalies do not match the conditions to maintain haze pollution.





210 **Figure 5.** Composite anomalies of (a-e) the spatial distribution of PM_{2.5} concentration (unit: $\mu\text{g m}^{-3}$)
 211 ³) from -3 days to 2 days related to Type1 severe HD_{EC} occur and (f-j) the corresponding horizontal
 212 wind (unit: m s^{-1}) at 500-hPa. (k-o) shows the zonal averaged PM_{2.5} concentration variations (unit:
 213 $\mu\text{g m}^{-3}$) and meridional wind variations (unit: m s^{-1}) in the range of 15-55°N, 105-135°E.
 214

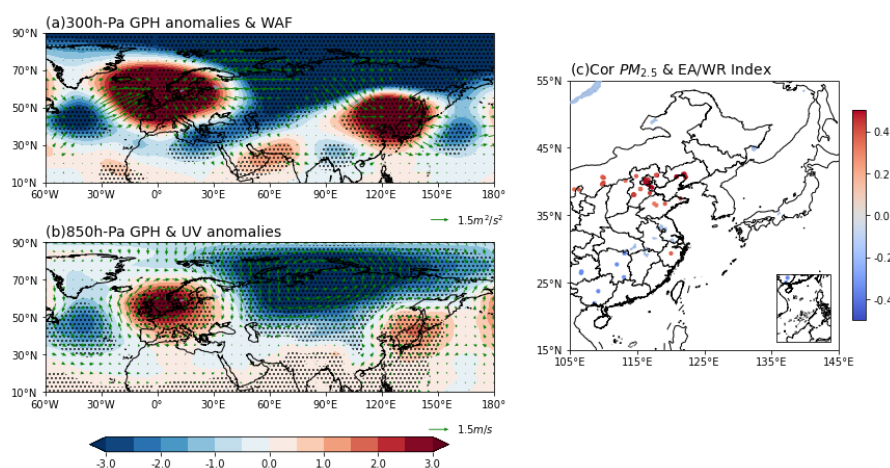
215 During the occurrence of circulation Type2, there was an anticyclonic anomaly with a quasi-
 216 barotropic structure over Northeast Asia, and the EC was located in the southwest of the anticyclone
 217 (Figure 6a, b, c). The significant positive TIP, sinking movement, and positive RH anomalies control
 218 the region over EC (Figure 6d, e, f). With the increase in TIP and the warm and humid air from the
 219 sea transports to the EC, the horizontal and vertical dispersion of pollutants was restrained, while
 220 higher surface RH exacerbated the formation of particulates. Such circulation anomalies are
 221 beneficial for the formation and maintenance of haze pollution.



222
 223 **Figure 6.** Composite anomalies of (a) GPH at 500-hPa (unit: gpm), horizontal wind (unit: m s^{-1}) at
 224 (b) 500-hPa and (c) 850-hPa, (d) TIP (unit: K), (e) omega (unit: $10^{-2} \text{ Pa s}^{-1}$), and (f) RH (unit: %)
 225 for circulation Type2. Dotted areas are statistically significant at the 95% confidence level.



226 Here we investigate the dynamic mechanism of the circulation Type2 by compositing the GPH
227 and WAF anomalies in the upper troposphere. The circulation anomalies show two quasi-zonal wave
228 trains over the mid-high latitudes. The one is characterized by a ‘-+-+’ pattern of GPH anomalies
229 from the south of Greenland across Siberia to Northeast China, with positive GPH anomalies in the
230 second and fourth centers. Such anomalies are similar to the positive phase of EA/WR
231 teleconnection, which can strengthen stable weather conditions over EC (Wu et al., 2016; Yin and
232 Wang, 2016) by causing weak wind speed, higher RH, and strong TIP (Niu et al., 2010; Ding and
233 Liu, 2014; Cai et al., 2017). Figure 7c shows the correlation coefficients between $PM_{2.5}$
234 concentration during the occurrence of circulation Type2 and the EA/WR index (The EA/WR index
235 was computed by the NOAA climate prediction center according to the rotated principal component
236 analysis used by Barnston and Livezey (1987)). The results show significant positive correlations
237 between the two in north EC and weak negative correlations in south EC. However, the circulation
238 Type2 caused the severe HD_{EC} for almost the whole EC, which is not completely consistent with
239 the results of Figure 7c. Therefore, we speculate that the other wave-train may lead to haze pollution
240 in south EC.



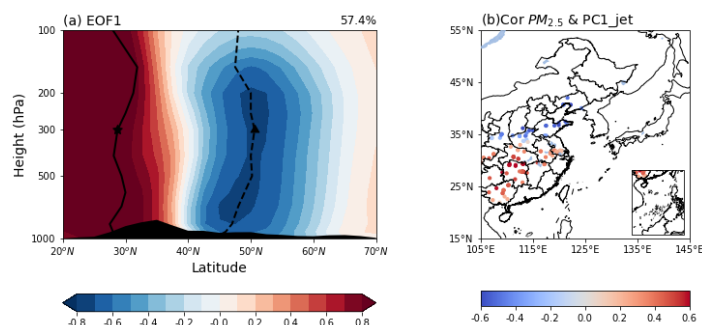
241
242 **Figure 7.** Composite anomalies of (a) GPH (shading; gpm) and WAF (vectors; $m^2 s^{-2}$) at 300-hPa,
243 and (b) GPH (shading; gpm) and horizontal wind (vectors; $m s^{-1}$) at 850-hPa for Type2. Dotted areas
244 are statistically significant at the 95% confidence level. (c) Correlation coefficients between Type2
245 $PM_{2.5}$ concentration and EA/WR index.

246



247 It can be found that the second wave-train reaches EC from Europe along with southern Asia,
248 forming a '+- + - +' pattern of GPH anomalies. The formation of such a wave-train is closely related
249 to the winter East Asia subtropical jet (EASJ) (Xiao et al., 2016; An et al., 2020; Zhang et al., 2022).
250 Here we use an Empirical orthogonal function (EOF) analysis of zonal wind from 1980 to 2021 to
251 determine the leading modes of winter EASJ (Xiao et al., 2016). The variance of the first mode
252 (EOF1) accounts for 57.4% of the total variance and indicates the intensity of EASJ (Figure 8a),
253 which could significantly affect the haze pollution in EC (An et al., 2020; Zhang et al., 2022).

254 The correlation coefficients between daily $PM_{2.5}$ concentration and the first principle component
255 ($PC1_{jet}$) during the occurrence of circulation Type2 is shown in Figure 8b, which has significant
256 positive correlations in south EC and negative correlations in north EC. It indicates that the
257 circulation Type2 may cause severe haze pollution in most areas of EC under the joint affection of
258 EA/WR teleconnection and winter EASJ. The results suggested that when discussing the impact of
259 an anticyclonic anomaly in Northeast Asia on haze pollution in EC, we should comprehensively
260 consider the joint affection of signals from high and middle latitudes.

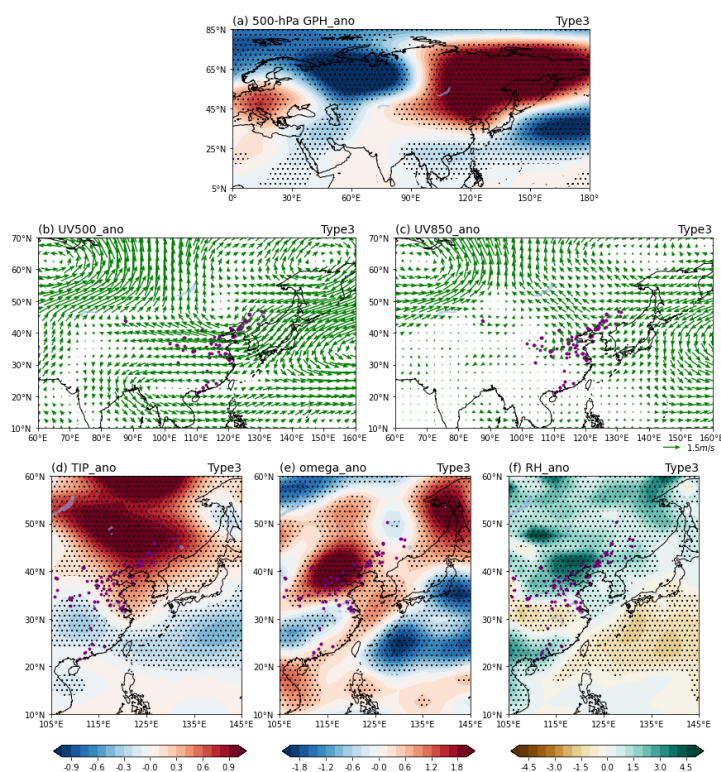


261
262 **Figure 8.** (a) The first EOF mode of zonal wind ($EOF1$, $m\ s^{-1}$) averaged from 60°E to 160°E in
263 NDJF. The star and circular at 300-hPa denote the subtropical jet and polar-front jet cores,
264 respectively. The zonal mean orography is dark-shaded. (b) Correlation coefficients between Type2
265 $PM_{2.5}$ concentration and $PC1_{jet}$.

266
267 Compared with circulation Type2, the range and intensity of anticyclonic anomalies in Northeast
268 Asia circulation Type3 are more robust, and the location is more northerly (Figure 9a). Such
269 circulation anomalies lead to southeasterly wind anomalies at 850-hPa, strong TIP, and abundant
270 moisture that induces severe haze over NEC (Figure 9d, f). In addition, the ascending motion over



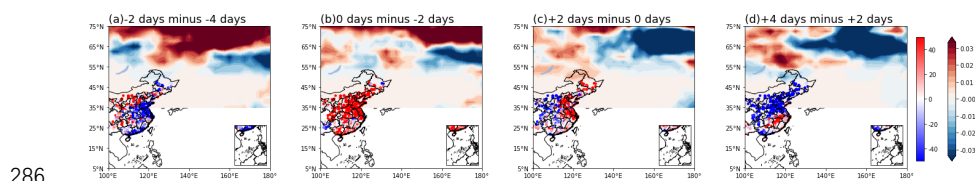
271 the south EC and the descending motion over the Beijing–Tianjin–Hebei region and NEC formed
272 meridional circulation cell anomalies (Figure 9e), which are conducive to the accumulation of
273 severe HD_{EC} over the NEC.



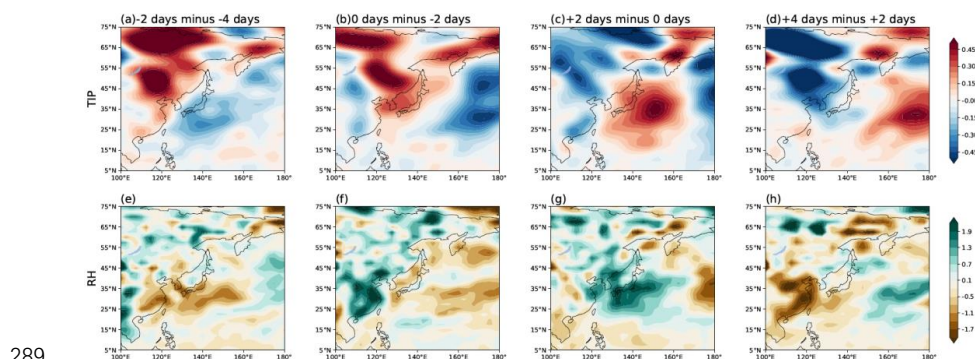
274
275 **Figure 9.** Composite anomalies of (a) GPH at 500-hPa (unit: gpm), horizontal wind (unit: m s^{-1}) at
276 (b) 500-hPa and (c) 850-hPa, (d) TIP (unit: K), (e) omega (unit: $10^{-2} \text{ Pa s}^{-1}$), and (f) RH (unit: %) for
277 circulation Type3. Dotted areas are statistically significant at the 95% confidence level.

278

279 In winter, the anticyclonic anomalies over the Okhotsk Sea are usually related to atmospheric
280 blocking (Yun and Yoo 2019; Fang et al., 2020; Hwang et al., 2022). Therefore, we calculated the
281 daily atmospheric blocking introduced in section 2.3 to investigate the relationship between Type3
282 severe HD_{EC}. Figure 10 shows that when Type3 severe HD_{EC} occurs, the PM_{2.5} concentration
283 increases with the blocking anomalies in the high-latitudes build-up, dissipating with the blocking
284 anomalies crash. The blocking anomalies strengthen the TIP and sufficient RH in the lower
285 atmosphere (Figure 11), causing severe HD_{EC} in NEC.



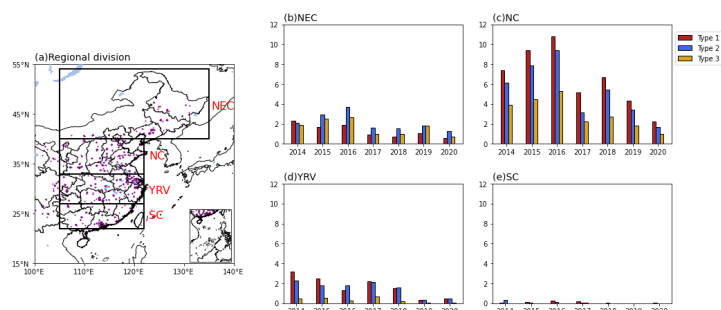
287 **Figure 10.** Composite anomalies of (a-d) the spatial distribution of PM_{2.5} concentration variations
288 (unit: $\mu\text{g m}^{-3}$) and blockings from -4 days to 4 days related to Type3 severe HD_{EC} occur.



290 **Figure 11.** Composite anomalies of (a-d) TIP variations (unit: K) and (e-h) RH variations (unit: %)
291 from -4 days to 4 days related to Type3 severe HD_{EC} occur.

292

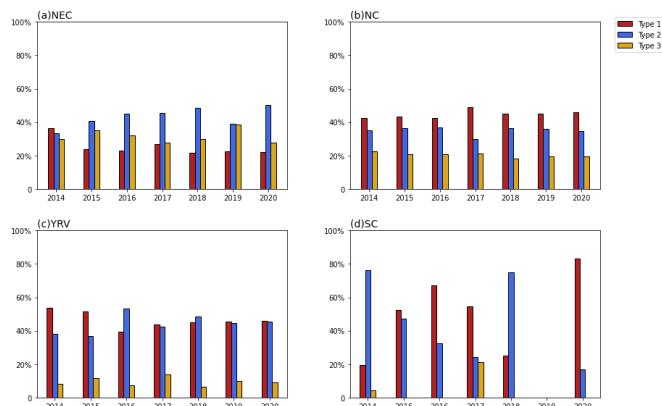
293 Based on the previous studies and the differences in the influence range of the three circulations
294 types in this study, we divided the EC into NEC (40°N-54°N, 105°E -135°E), North China (NC;
295 33°N-40°N, 105°E -122°E), the YRV (27°N-33°N, 105°E -122°E), and SC (22°N-27°N, 105°E -
296 122°E) to analyze the temporal characteristics of three HD_{EC} types in different subregions of EC
297 (Figure 12a). Figure 12b, c, d, and e display the annual regional averaged frequency of the three
298 HD_{EC} types in the four subregions. The results show that severe haze pollution mainly occurs in NC
299 and less in SC. The frequency of severe haze generally shows a downward trend in the four
300 subregions.



301
302 **Figure 12.** (a) The four subregions of EC. The purple dots are the stations. (b-e) Frequency of three
303 types of cool season severe HD_{EC} in NEC, NC, YRV, and SC.

304

305 We further calculated the proportion of the frequency of each circulation type in the total annual
306 severe haze frequency in the four subregions (Figure 13). For NEC, the proportion of the three
307 circulation types is almost equal. It should be noted that the proportion of the circulation Type3
308 is much larger than that in the other three subregions. In NC, the proportion of the circulation Type1
309 is more than 40%, while the proportion of the circulation Type3 is about 20%. For YRV, circulation
310 Type1 and Type2 lead the severe haze pollution. There are relatively few severe haze pollution in
311 SC. Therefore, the dominant circulation type in SC has strong interannual variation and is hardly
312 affected by the circulation Type3. Overall, on the weather scale, the HD_{EC} is affected by a variety
313 of synoptic circulations, and the areas affected by each synoptic circulation are also different.



314

315 **Figure 13.** Annual percentage of the three types of severe HD_{EC} in (a) NEC, (b) NC, (c) YRV, and
316 (d) SC.



317 5. Conclusions and discussion

318 In this study, the Hierarchical Clustering Algorithm was used to investigate three dominant
319 circulation types that could lead to severe HD_{EC} . We cluster the circulations over the stations in EC
320 on the severe haze days from 2014 to 2021, which eliminates the interference of the circulations of
321 non-severe haze days on the cluster results. The results show that three dominant circulation types
322 associated with severe HD_{EC} are obtained, which are mainly characterized by a local anticyclonic
323 anomaly but also present obvious spatial variation on large scale circulations. The circulation Type1
324 with wave-train structure of “-+-” in the upper troposphere mainly causes severe haze pollution in
325 the YRV through the low-level north wind anomalies over NC. Although the sinking movement,
326 TIP, and RH anomalies over the YRV are weak or not significant, the regional haze transportation
327 leads to the severe haze in the YRV. The circulation Type2 is characterized by two quasi-barotropic
328 Rossby wave trains at 300-hPa, which may be stimulated and sustained by the joint affection of
329 EA/WR teleconnection and the winter EASJ. One travels from the south of Greenland across Siberia
330 to NEC, forming a ‘-++’ pattern of GPH anomalies, and the other travels from Europe along with
331 southern Asia, forming a ‘+-+’ pattern of GPH anomalies, which led an anticyclonic over
332 northeastern Asia and conducive to the accumulation of haze. The circulation Type3 is characterized
333 by blocking anomaly over Okhotsk Sea, which influences the severe HD_{EC} over NEC with
334 southeasterly wind at 850-hPa, strong TIP, and abundant moisture. The temporal characteristics of
335 three circulation types in NEC, NC, YRV, and SC were further analyzed. The result shows that on
336 the synoptic scale, HD_{EC} is affected by various synoptic atmospheric circulations, and the regions
337 affected by each synoptic atmospheric circulation are also different.

338 The study shows that circulation patterns and key systems that contribute to severe HD_{EC} are
339 complex and diverse revealing the dominant circulation patterns of severe haze in different regions
340 of EC. These three dominant atmospheric circulation patterns could be potentially used to establish
341 severe winter haze prediction models for different regions of EC (e.g., project the future variations
342 of severe haze in different regions of EC by identifying similar circulation patterns through machine
343 learning or regression fitting). Due to the limitation of data, it is difficult to carry out the work of
344 circulation classification over a longer period. Therefore, whether there is an interannual or
345 interdecadal connection between the dominant circulation types of severe haze and its key
346 circulation system needs further investigation. This study shows that different circulation types may
347 lead to severe haze in different regions of EC, and further studies are needed to investigate whether



348 there are differences in persistence or intensity among them.

349 **Data availability**

350 The Daily PM_{2.5} concentrations for 935 meteorological stations in China are collected by the
351 China National Environmental Monitoring Centre archive at: <https://quotsoft.net/air/> (last access:
352 16 May 2022). Daily mean meteorological data are obtained from the NCEP/NCAR reanalysis data
353 archive at: <https://psl.noaa.gov/data/gridded/data.ncep.reanalysis.pressure.html> (last access: 16
354 May 2022, NCEP/NCAR, 2022). The monthly EA/WR Index (CPC, 2022) can be downloaded from
355 NOAA's Climate Prediction Center: <http://www.cpc.ncep.noaa.gov/data/teledoc/telecontents.shtml>
356 (last access: 16 May 2022).

357 **Competing interests**

358 The authors declare that they have no conflict of interest.

359 **Author contributions**

360 SZ and GZ put forward the conception of this paper, TW improved the research and manuscript.
361 SZ, XY and IV performed research. SZ wrote the manuscript with contributions from all co-authors.

362 **Acknowledgments**

363 This research is supported by the National Natural Science Foundation of China (42175035 and
364 42077192) and the Postgraduate Research & Practice Innovation Program of Government of Jiangsu
365 Province (KYCX22_1162).

366 **References**

367 An, X., Sheng, L., Liu, Q., Li, C., Gao, Y., Li, J.: The combined effect of two westerly EAJS
368 waveguides on heavy haze in the North China plain in November and December 2015. Atmos.
369 Chem. Phys. 20 (8), 4667–4680. <https://doi.org/10.5194/acp-20-4667-2020>, 2020.



- 370 Barnston, A. G. and Livezey, R. E.: Classification, seasonality and persistence of low frequency
371 atmospheric circulation patterns, *Mon. Weather Rev.*, 115, 1083–1126, 1987.
- 372 Cai, W. J., Li, K., Liao, H., Wang, H. J., and Wu, L. X.: Weather Conditions Conducive to Beijing
373 Severe Haze More Frequent under Climate Change, *Nat. Clim. Change*, 7, 257–262,
374 <https://doi.org/10.1038/nclimate3249>, 2017.
- 375 Cai, W., Xu, X., Cheng, X., Wei, F., Qiu, X., and Zhu, W.: Impact of “blocking” structure in the
376 troposphere on the wintertime persistent heavy air pollution in northern China, *Sci. Total Environ.*,
377 741, 140325, <https://doi.org/10.1016/j.scitotenv.2020.140325>, 2020.
- 378 Chen, H. P., Wang, H.J.: Haze Days in North China and the associated atmospheric circulations
379 based on daily visibility data from 1960 to 2012, *Journal of Geophysical Research: Atmospheres*,
380 120(12), 5895–5909, <https://doi.org/10.1002/2015JD023225>, 2015.
- 381 Ding, X., Zhang, Y.Q., He, Q.F., Yu, Q.Q., Shen, R.Q., Zhang, Y.L., Zhang, Z., Lyu, S.J., Hu, Q.H.,
382 Wang, Y.S., Li, L.F., Song, W., Wang, X.M.: Spatial and seasonal variations of secondary organic
383 aerosol from terpenoids over China. *J. Geophys. Res. Atmos.*, 121, 14661–14678,
384 <https://doi.org/10.1002/2016JD025467>, 2016.
- 385 Ding, Y. H., and Liu, Y. J.: Analysis of long-term variations of fog and haze in China in recent 50
386 years and their relations with atmospheric humidity, *Sci. China Ser. D: Earth Sci.*, 57, 36–46,
387 <https://doi.org/10.1007/s11430-013-4792-1>, 2014.
- 388 Fan, X. Q., Sun, Z. B: Analysis on Features of Haze Weather in Xiamen City during 1953–2008.
389 *Trans. of Atmos. Sci.* 32, 604–609, 2019.
- 390 Fang, B., & Lu, M.: Heatwave and blocking in the Northeastern Asia: Occurrence, variability, and
391 association, *Journal of Geophysical Research: Atmospheres*, 125, e2019JD031627.
392 <https://doi.org/10.1029/2019JD031627>, 2020.
- 393 Hu, B., Chen, R., Xu, J. X., Yang, G. S., Xu, D. D., Chen, C. Y., and Zhao, Y. L.: Health effects of
394 ambient ultrafine (nano) particles in haze, *Chinese Sci. Bull.*, 60, 2808–2823,
395 <https://doi.org/10.1360/N972014-01404>, 2015 (in Chinese).
- 396 Hwang, J., Son, SW., Martineau, P., Barriopedro, D.: Impact of winter blocking on surface air
397 temperature in East Asia: Ural versus Okhotsk blocking, *Climate Dynamics*,
398 <https://doi.org/10.1007/s00382-022-06204-5>, 2022.



- 399 Kalnay, E., Kanamitsu, M., Kistler, R., Collins, W., Deaven, D., Gandin, L., Iredell, M., Saha, S.,
400 White, G., Woollen, J., Zhu, Y., Leetmaa, A., Reynolds, R., Chelliah, M., Ebisuzaki, W., Higgins,
401 W., Janowiak, J., Mo, K. C., Ropelewski, C., Wang, J., Jenne, R., Joseph, D., The NCEP/NCAR
402 40-year reanalysis project. *B. Am. Meteorol. Soc.*, 77, 437–471, [https://doi.org/10.1175/1520-](https://doi.org/10.1175/1520-0477(1996)077b0437:TNYRPN2.0.CO;2)
403 [0477\(1996\)077b0437:TNYRPN2.0.CO;2](https://doi.org/10.1175/1520-0477(1996)077b0437:TNYRPN2.0.CO;2), 1996.
- 404 Leung, D. M., Tai, A. P. K., Mickley, L. J., Moch, J. M., van Donkelaar, A., Shen, L., and Martin,
405 R. V.: Synoptic meteorological modes of variability for fine particulate matter (PM_{2.5}) air quality
406 in major metropolitan regions of China, *Atmos. Chem. Phys.*, 18, 6733–6748,
407 <https://doi.org/10.5194/acp-18-6733-2018>, 2018.
- 408 Li, J., Liao, H., Hu, J., and Li, N.: Severe particulate pollution days in China during 2013–2018 and
409 the associated typical weather patterns in Beijing-Tianjin-Hebei and the Yangtze River Delta
410 regions, *Environ. Pollut.*, 248, 74–81, 2019.
- 411 Li, K., Jacob, D. J., Liao, H., Qiu, Y. L., Shen, L., Zhai, S. X., Bates, K. H., Sulprizio, M. P., Song,
412 S. J., Lu, X., Zhang, Q., Zheng, B., Zhang, Y. L., Zhang, J. Q., Lee, H. C., Kuk, S. K.: Ozone
413 pollution in the North China Plain spreading into the late-winter haze season, *Proceedings of the*
414 *National Academy of Sciences*, 118(10): e2015797118, <https://doi.org/10.1073/pnas.2015797118>,
415 2022.
- 416 Li, Q., Zhang, R. H., and Wang, Y.: Interannual variation of the winter-time fog–haze days across
417 central and eastern China and its relation with East Asian winter monsoon. *Int. J. Climatol.*, 36,
418 346–354, <https://doi.org/10.1002/joc.4350>, 2015.
- 419 Liu, X., Hui, Y., Yin, Z. Y., Wang, Z., Xie, X., Fang, J.: Deteriorating haze situation and the severe
420 haze episode during December 18–25 of 2013 in Xi’an China, the worst event on record, *Theor.*
421 *Appl. Climatol.*, <https://doi.org/10.1007/s00704-015-1509-8>, 2015.
- 422 Monks, P., Granier, C., Fuzzi, S., Stohl, A., Williams, M., Akimoto, H., Amann, M., Baklanov, A.,
423 Baltensperger, U., Bey, I.: Atmospheric composition change–Global and regional air quality,
424 *Atmos. Environ.*, 43, 5268–5350, <https://doi.org/10.1016/j.atmosenv.2009.08.021>, 2009.
- 425 Niu, F., Li, Z. Q., Li, C., Lee, K. H., Wang, M. Y.: Increase of wintertime fog in China: Potential
426 impacts of weakening of the eastern Asian monsoon circulation and increasing aerosol loading, *J.*
427 *Geophys. Res.*, 115, D00K20, <https://doi.org/10.1029/2009JD013484>, 2010.



- 428 Plumb, R.A.: On the three-dimensional propagation of stationary waves, *J. Atmos. Sci.*, 42, 217–
429 229, [https://doi.org/10.1175/1520-0469\(1985\)042<0217:OTTDPO.2.0.CO;2](https://doi.org/10.1175/1520-0469(1985)042<0217:OTTDPO.2.0.CO;2), 1985.
- 430 Qian, Y., Gong, D., Fan, J., Leung, L.R., Bennartz, R., Chen, D., Wang, W.: Heavy pollution
431 suppresses light rain in China: Observations and modeling, *J. Geophys. Res.*, 114,
432 <https://doi.org/10.1029/2008JD011575>, 2009.
- 433 Rokach, L., Maimon, O.: Clustering methods. *Data mining and knowledge discovery handbook*,
434 Springer US, 321-352, 2005.
- 435 Rousseeuw, P.: Silhouettes: A graphical aid to the interpretation and validation of cluster analysis.
436 *Journal of Computational and Applied Mathematics*, 20, 5365, [https://doi.org/10.1016/0377-](https://doi.org/10.1016/0377-0427(87)90125-7)
437 [0427\(87\)90125-7](https://doi.org/10.1016/0377-0427(87)90125-7), 1987.
- 438 Shen, L., Jacob, D. J., Mickley, L. J., Wang, Y., and Zhang, Q.: Insignificant effect of climate change
439 on winter haze pollution in Beijing, *Atmos. Chem. Phys.*, 18, 17489–17496,
440 <https://doi.org/10.5194/acp-18-17489-2018>, 2018.
- 441 Shi, C., Zhang, H., Roth, M., Li, Z.: Impacts of urbanization on long-term fog variation in Anhui
442 Province, China. *Atmos. Environ.*, 42, 8484–8492, <https://doi.org/10.1016/j.atmosenv.2008.08.002>,
443 2008.
- 444 Sun, Y., Chen, C., Zhang, Y., Xu, W., Zhou, L., Cheng, X., Zheng, H., Ji, D., Li, J., Tang, X., Fu, P.,
445 Wang, Z.: Rapid formation and evolution of an extreme haze episode in Northern China during
446 winter 2015, *Sci. Rep.* 6, 27151, <https://doi.org/10.1038/srep27151>, 2016.
- 447 Sun, Y., Ma, Z. F., Niu, T.R., Fu, Y., Hu, J.F.: Characteristics of climate change with respect to fog
448 days and haze days in China in the past 40 years. *Clim. Environ. Res.*, 18, 397–406, 2013.
- 449 Tibaldi, S., and F. Molteni: On the operational predictability of blocking. *Tellus*, 42A, 343–365, 1990.
- 450 Tsaia, F., Tu, J. Y., Hsu, S. C., Chen, W. N.: Case study of the Asian dust and pollutant event in
451 spring 2006: Source, transport, and contribution to Taiwan, *Sci. Total Environ.*, 478, 163–174,
452 <https://doi.org/10.1016/j.scitotenv.2014.01.072>, 2014.
- 453 Wang, H. J., Chen, H. P., Liu, J. P.: Arctic Sea Ice Decline Intensified Haze Pollution in Eastern
454 China. *Atmos. Oceanic Sci.*, 8:1, 1-9, <https://doi.org/10.3878/AOSL20140081>, 2015.
- 455 Wang, K. C., Dickinson, R. E., Liang, S. L.: Clear sky visibility has decreased over land globally
456 from 1973 to 2007, *Science*, 323, 1468–1470, <https://doi.org/10.1126/science.1167549>, 2009.



- 457 Wang, X. Y., Zhang, R. H., Tan, Y. K., Yu, W.: Dominant synoptic patterns associated with the decay
458 process of PM_{2.5} pollution episodes around Beijing, *Atmos. Chem. Phys.*, 21, 2491–2508,
459 <https://doi.org/10.5194/acp-21-2491-2021>, 2021.
- 460 Wang, X.Y., Dickinson, R.E., Su, L.Y., Zhou, C.L., Wang, K.C.: PM_{2.5} pollution in China and how
461 it has been exacerbated by terrain and meteorological conditions, *Bulletin of the American*
462 *Meteorological Society*, 99(1): 105-119, <https://doi.org/10.1175/BAMS-D-16-0301.1>, 2018.
- 463 Wang, X.Y., Zhang, R.H., Effects of atmospheric circulations on the interannual variation in PM_{2.5}
464 concentrations over the Beijing–Tianjin–Hebei region in 2013–2018, 20, 7667–7682,
465 <https://doi.org/10.5194/acp-20-7667-2020>, 2020.
- 466 Wang, Z.S., Liu, X.D., Xie, X.N.: Effects of Strong East Asian Cold Surges on Improving the Air
467 Quality over Mainland China, *Atmosphere*, 7, 38, <https://doi.org/10.3390/atmos7030038>, 2016.
- 468 Wei, Y., Li, J., Wang, Z., Chem, H., Wu, Q., Li, J., Wang, Y., and Wang, W.: Trends of surface PM_{2.5}
469 over Beijing–Tianjin–Hebei in 2013–2015 and their causes: emission controls vs. meteorological
470 conditions, *Atmos. Oceanic Sci. Lett.*, 10, 276–283,
471 <https://doi.org/10.1080/16742834.2017.1315631>, 2017.
- 472 Wu, M., Wu, D., Fan, Q., Wang, B. M., Li, H. W., Fan, S. J.: Observational studies of the
473 meteorological characteristics associated with poor air quality over the Pearl River Delta in China,
474 *Atmos. Chem. Phys.* 13, 10755–10766, <https://doi.org/10.5194/acp-13-10755-2013>, 2013.
- 475 Wu, P., Ding, Y. H., Liu, Y. J., and Li, X. C.: Influence of the East Asian winter monsoon and
476 atmospheric humidity on the wintertime haze frequency over central-eastern China, *Acta Meteorol.*
477 *Sin.*, 74, 352–366, <https://doi.org/10.11676/qxxb2016.029>, 2016 (in Chinese).
- 478 Wu, P., Ding, Y., and Liu, Y.: Atmospheric circulation and dynamic mechanism for persistent haze
479 events in the Beijing–Tianjin–Hebei region, *Adv. Atmos. Sci.*, 34, 429–440, 2017.
- 480 Xiao, C., Zhang, Y., Lofgren, B. M., & Nie, Y.: The concurrent variability of East Asian subtropical
481 and polar-front EAJs and its implication for the winter climate anomaly in China, *Journal of*
482 *Geophysical Research: Atmospheres*, 121(12), 6787–6801, 2016.
- 483 Xie, Y. B., Chen, J., and Li, W.: An assessment of PM_{2.5} related health risks and impaired values
484 of Beijing residents in a consecutive high-level exposure during heavy haze days, *Environ. Sci.*,
485 35, 1–8, 2014.



- 486 Xu, J., Yan, F., Xie, Y., Wang, F., Wu, J., Fu, Q.: Impact of meteorological conditions on a nine-day
487 particulate matter pollution event observed in December 2013, Shanghai, China, *Particuology*, 20,
488 69–79, <https://doi.org/10.1016/j.partic.2014.09.001>, 2015.
- 489 Yin, Z. C. and Wang, H. J.: The relationship between the subtropical Western Pacific SST and haze
490 over North-Central North China Plain, *Int. J. Climatol.*, 36, 3479–3491,
491 <https://doi.org/10.1002/joc.4570>, 2016.
- 492 Yin, Z. C., Wang, H. J., and Chen, H. P.: Understanding severe winter haze events in the North
493 China Plain in 2014: roles of climate anomalies, *Atmos. Chem. Phys.*, 17, 1641–1651,
494 <https://doi.org/10.5194/acp-17-1641-2017>, 2017.
- 495 Yin, Z. C., Wang, H. J., and Yuan, D. M.: Interdecadal increase of haze in winter over North China
496 and the Huang-huai area and the weakening of the East Asia winter monsoon. *Chin. Sci. Bull.*, 60,
497 1395–1400, 2015
- 498 Yin, Z. C., Wang, H. J.: Possible Relationship between the Chukchi Sea Ice in the Winter and the
499 February Haze Pollution in the North China Plain, *Journal of Climate*, 32(16), 5179–5190,
500 <https://doi.org/10.1175/JCLI-D-18-0634.1>, 2019.
- 501 Yin, Z. C., Wang, H. J.: Role of atmospheric circulations in haze pollution in December 2016,
502 *Atmospheric Chemistry and Physics*, 17(18): 11673–11681, [https://doi.org/10.5194/acp-17-11673-](https://doi.org/10.5194/acp-17-11673-2017)
503 [2017](https://doi.org/10.5194/acp-17-11673-2017), 2017.
- 504 Yin, Z. C., Zhang, Y.J., Wang, H.J., Li, Y.Y., Evident PM_{2.5} drops in the east of China due to the
505 COVID-19 quarantine measures in February, *Atmospheric Chemistry and Physics*, 21, 1581–1592,
506 <https://doi.org/10.5194/acp-21-1581-2021>, 2021.
- 507 Yun, S., Yoo, C.: The effects of spring and winter blocking on PM10 Concentration in Kore,
508 *Atmosphere*, 10(7): 410, <https://doi.org/10.3390/atmos10070410>, 2019.
- 509 Zhang, S.Y., Zeng, G., Yang, X.Y., Wu, R.X., Yin, Z.C.: Comparison of influence between two types
510 of cold surge on haze dispersion in Eastern China, *Atmospheric Chemistry and Physics*, 21, 15185–
511 15197, <https://doi.org/10.5194/acp-21-15185-2021>, 2021.
- 512 Zhang, S.Y., Zeng, G., Wang, T.J., Yang, X.Y., Vedaste, I.: Interannual relationship between
513 displacement and intensity of East Asian jet stream and haze over eastern China in winter, *Science*



514 of the Total Environment, <http://dx.doi.org/10.1016/j.scitotenv.2022.154672>, 2022.

515 Zhong, W. G., Yin, Z. C., Wang, H. J.: The relationship between anticyclonic anomalies in

516 northeastern Asia and severe haze in the Beijing–Tianjin–Hebei region, *Atmos. Chem. Phys.*, 19,

517 5941–5957, <https://doi.org/10.5194/acp-19-5941-2019>, 2019.